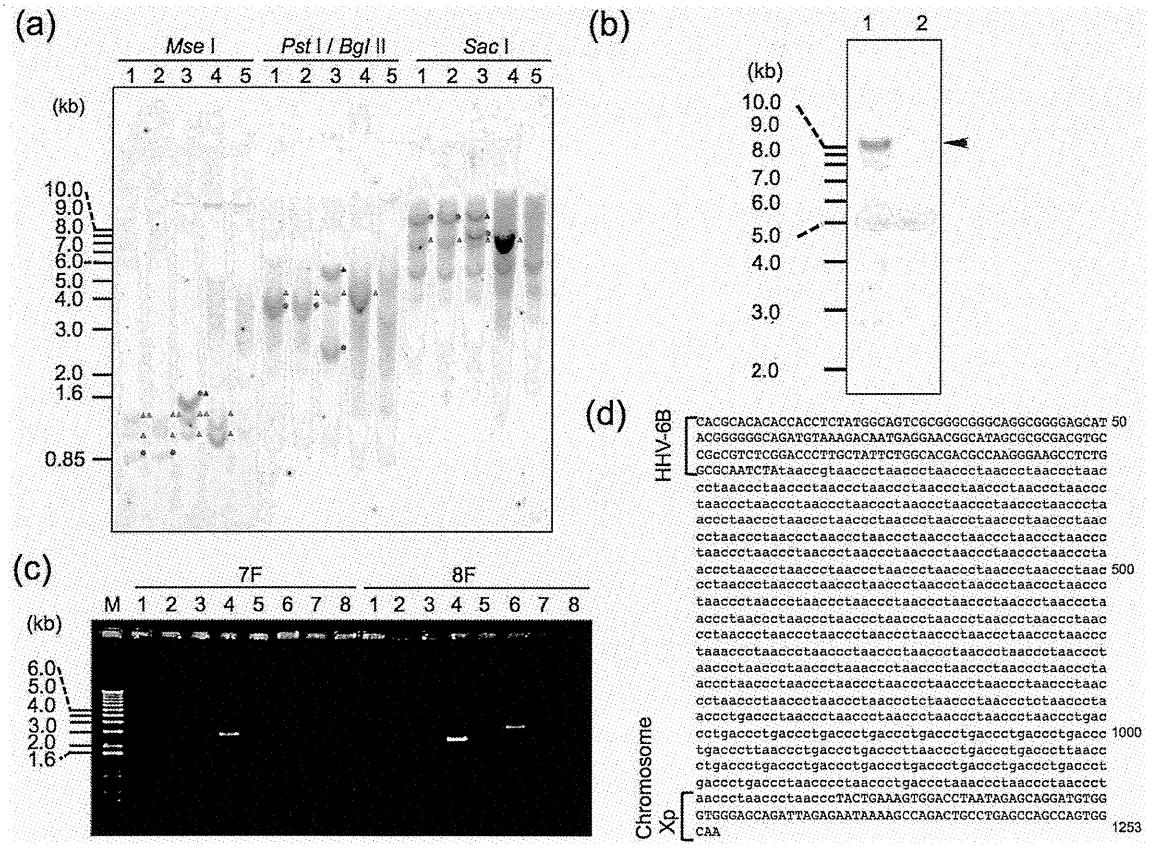

Figure 3 | Analyses of the junction between the human chromosome and viral genome. (a) Southern blot analyses of genomic DNA from the CIHHV-6B study subjects. The restriction enzymes used for these analyses are indicated above the panels; size markers are indicated on the left. Red dots indicate the rearranged bands derived from junction between human telomere and the HHV-6. Triangles indicate bands derived from the DR-L (green) and DR-R (orange), while blue triangles indicate the junction of the two DRs. Lane 1, case 18; lane 2, case 19; lane 3, case 28; lane 4, case 31; lane 5, non-CIHHV-6 control. (b) Southern blot analyses of PCR products. The arrowhead indicates a junction-specific PCR product. Lane 1, case 28; lane 2, non-CIHHV-6. Complete raw autoradiogram image can be seen in Supplementary Fig. S6. (c) PCR products that incorporate junction fragments. The primer sets were designed on the DR region (7F or 8F) and subtelomeric region on chromosomes X. Two CIHHV-6 cases yielded amplicons of different sizes. Lane M, size markers; lane 1, case 18; lane 2, case 19; lane 3, case 20; lane 4, case 28; lane 5, case 31; lane 6, case 63; lane 7, non-CIHHV-6 case; lane 8, water control. (d) Sequence of the junctions in case 28. The sequence shown covers the region from the DR-R of the viral genome to the human subtelomeric region. Lowercase letters denote telomere repeats.

in all cases (Supplementary Fig. S2b). We next performed PCR using one fixed primer for the site just outside of the DR-L and other primers for different sites within the DR. All of the primers within the DR successfully amplified specific products (Fig. 4). A telomere-repeat primer also yielded products appearing as a smear, the specificity of which was confirmed by Southern hybridization (Supplementary Fig. S5b). However, the use of a primer for the pac1 site did not yield any specific product. We also designed MLPA probes within the pac1 or pac2 region which produced a single copy signal which was similar to the UL region (Fig. 2), suggesting the absence of the pac1 site. These results demonstrated that the CIHHV-6B chromosome ends within the TRS-1.

The presence of the TRS-2 in the DR-L not only indicated an intact TRS-2, but also gave us the opportunity to analyze individual variations in the TTAGGG repeat numbers. As expected, the sizes of the PCR products varied among individuals (Supplementary Fig. S2b)[21]. Among three of our study subjects with an integration at 22q, two cases from the same family (cases 19 and 20) showed an amplified product of the same size. The other case with a viral integration at 22q (case 18) showed a PCR product of a similar size but subsequent sequence analysis revealed different numbers of telomere repeats (32 for cases 19 and 20 versus 29 for case 18). Two cases with a viral integration at Xp showed different numbers of repeats (27 for case 28 and 23 for case 63).

Discussion

In our present study, we analyzed the structure of the integrated HHV-6B genome in six carriers of this virus using the MLPA technique. Achieving accuracy in copy number measurements poses particular challenges when attempting to characterize a tandem repeat region. The MLPA method shows utility in reproducibly distinguishing two copies of repeats from a single copy, which is not easily achievable using other standard methods. MPLA also overcomes the instability of the qPCR technique due to its high sensitivity to the amounts of template DNA, and thereby yields reproducible results[22]. Hence, MLPA is often used for the identification of deletion/duplication mutations in disease-causing genes or for determining the status of copy number variations at certain chromosomal loci in humans. In our current study, the use of MLPA allowed us to clearly determine the copy number of the integrated HHV-6B genome in the carriers and to characterize structural variations in the integrated viral genome among these CIHHV-6B cases. Our data indicate that human telomere repeats and the viral genomes had fused via one of the two TRSs within the DR-R in all six cases and

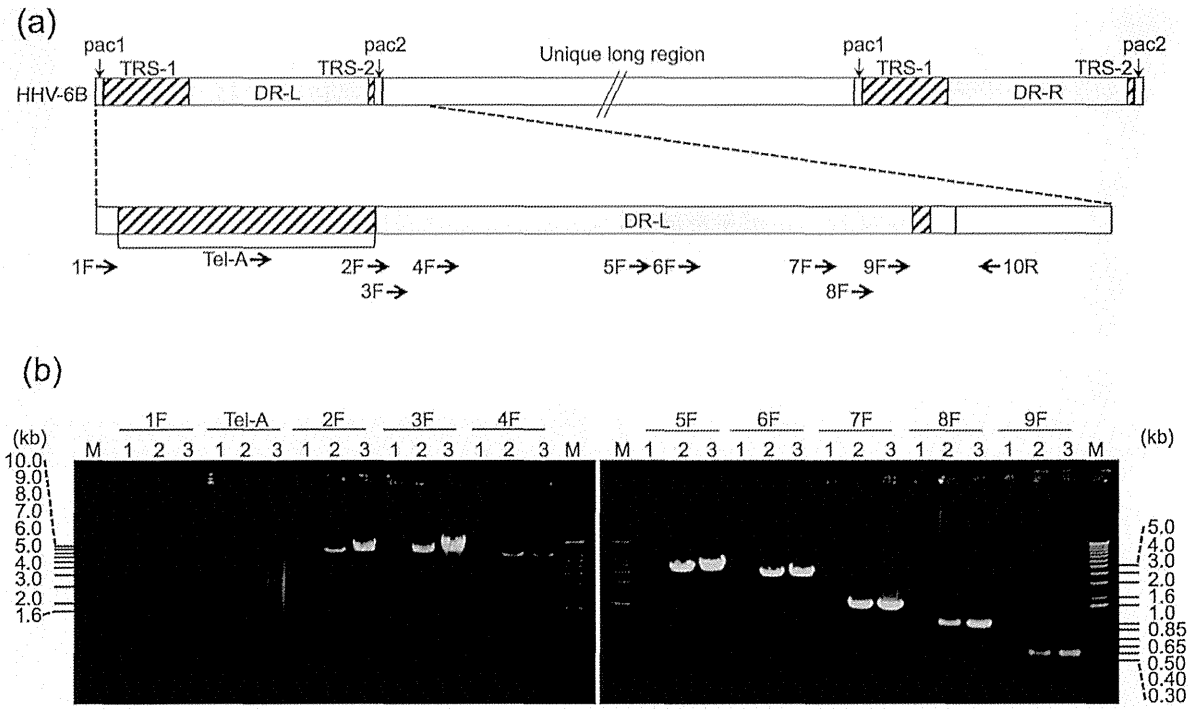

Figure 4 | Long range PCR analyses to determine the endpoints of the viral genomes. (a) Schematic representation of the HHV-6B genomic structure. The positions of the PCR primers are indicated below the diagram. (b) Results of long range PCR analyses. The 10R primer was used together with one of the DR primers for the long range PCR. The DR primers are indicated above the panels. Lane M, size markers; lane 1, non-CIHHV-6 case; lane 2, case 28; lane 3, case 18.

that the other end of the integrated HHV-6 virus is likely to be the distal TRS within the DR-L. Our findings are almost similar to those published previously[18,25]. These data implicate dual roles for the viral TRS sites in the manifestation of CIHHV-6.

The first important role of the viral TRS in the onset of CIHHV-6 is to trigger the homology-directed DNA repair mechanism for subsequent integration of the viral genome into the human genome. The ends of chromosomal DNA comprising the telomeres are generally structurally organized not to activate a DNA damage response by forming a stable T-loop DNA secondary structure and through the assembly of a shelterin complex[17]. Indeed, in normal cells, homologous recombination is repressed at the telomere[23]. However, the shortening of telomeres as a result of cell division might lead to a loss of chromosomal end protection and may cause improper DNA repair such as end-to-end fusions of the chromosomes by non-homologous end joining[24]. In our current study, the telomere repeats at the junction between the human subtelomere and the HHV-6 genome were found to be low in number, which has also been reported previously[18]. We thus speculate that telomere shortening, when it occurs in the cells infected with HHV-6, may activate a homology-directed DNA damage response that leads to viral integration.

A previous report has indicated that the viral breakpoints are located at TRS-2, both for CIHHV-6A and 6B[18,25]. The TRS-2 site has been shown to be longer and contain fewer degenerate TTAGGG repeats than TRS-1. However, our current analyses has revealed that the sizes of the TRS-1 region in our study subjects were much larger than TRS-2 and contained more perfect telomere repeats. If the free DNA end at the human telomere had activated the homology-directed DNA repair response pathway and searched for the appropriate template for DNA repair via homology, the integration event would have preferentially utilized TRS-1. However, we found that this was not the case. Thus, we speculate that the viral DNA end may be recognized as a bona fide DNA end by the host DNA repair system and thus subjected to end resection via homology-directed machinery. A small resection would be sufficient to reach the TRS-2 in the DR-R and enable the DNA end to find its homologous template, i.e. the human telomere. If the protection of the human telomere is incidentally removed at the time of this homology search due to age-related telomere shortening, the two DNA ends might be connected in a homology-dependent manner.

Once HHV-6 infection is established, the circularization of the linear double stranded viral DNA give rises to the formation of a stable episomal form in the nucleus whereby latency is achieved[26]. During HHV-6 replication, the episome produces a head-to-tail concatemer via a rolling circle mechanism, which is cleaved into a single unit of linear viral genome and is subsequently recircularized. A previous study has reported that some CIHHV individuals carry more than two copies of HHV[27]. However, in our current study we found only one copy of the viral genome in all of the CIHHV-6 cases in our cohort. In case 28, we identified tandem DRs repeat with no intervening pac1-pac2 region, which should be identified in a replicating concatemer or episomal virus. This suggests that a single linear form of replicated HHV-6 in latently infected cells gives rise to the integration event[10]. Normally, linear viral DNA ends are protected by episome formation, but it is possible that replication errors at the junction might result in an uncircularized virus genome, which may induce a DNA damage response. Although homologous recombination is suppressed at the telomere, a recent report has provided evidence of single strand annealing as a mechanism of telomere fusion[28].

The second pivotal role of the TRS regions in CIHHV-6 is the stabilization of the chromosomal end required for transmission of the virus. In our current analyses, we demonstrate that the end of the HHV-6B integrated chromosome was TRS-1, which others have also demonstrated using single telomere length analyses[25]. Once HHV-6 is integrated into the human telomere via homology with the TRS in the DR-R, the other end of the viral genome, DR-L, becomes a chromosomal end. Without the protection that normally operates

Table 1 | Characteristics of the Japanese study subjects with CIHHV-6B

Family	Case	Trigger for the diagnosis of CIHHV-6B	Chromosome
1	18	Monitoring after bone-marrow transplantation Aplastic anemia	22q
2	19	Differential diagnosis of mycoplasma Encephalitis	22q
	20	Mother of case19	22q
3	28	Monitoring after bone-marrow transplantation Congenital pure red cell aplasia	Xp
4	31	Differential diagnosis of febrile skin rash	6q
5	63	Uveitis	Xp

for chromosomal ends at the telomeres, the DR-L is subject to DNA end resection until the TRS-1 appears. Since the TRS-1 length is sufficient to recruit components of the shelterin complex, it can form a neo-telomere to maintain its size during some rounds of DNA replication and cell division until it forms gametes to transmit the viral genome to the offspring. We note that there is no reported case of chromosomally integrated HHV-7[29] and this might be due to a short TRS-1 (90 bp) in the genome of this virus which cannot maintain chromosomal end stabilization (U43400).

One of our current CIHHV-6B cases (case 31) was found to carry a different junction between the virus and human telomere, with a breakpoint in the TRS-1 region. One possibility for this occurrence is that a long DNA end resection took place that extended to the TRS1, which may be rare. Another possibility is a post-insertional genomic rearrangement[30]. Alternatively, non-allelic homologous recombination (NAHR) between the two TRS sites might have produced the deletion of DR-R in case 31, thereby mimicking the breakpoint at a different location for the initial integration. Another CIHHV-6B subject in our present analyses (case 28) was found to carry three DR copies. This is also possibly a product of an NAHR event between the two different TRS sites on the HHV-6 virus. In contrast to the normal repression of homologous recombination at the telomere, the subtelomeric region is known to be highly unstable and undergo frequent recombination[31]. The integration of HHV-6B in cases 28 and 63 in our present study are likely to have originated from a single ancestor since an identical genomic structure, three DR sites without a pac1-pac2 junction, was found in these two individuals. However, the repeat number at the TRS2-human telomere junction, as well as in the TRS2 site at the DR-L was found to be diverse between these two cases, suggesting that replication slippage or recombination may occur frequently at this new subtelomeric region.

A remaining question from our current observations is the timing of HHV-6 integration during the life cycle of a human host. Since CIHHV-6 appears to be transmitted from parent to child in a Mendelian fashion, the integration event must occur during germ cell development. HHV-6 uses CD46 as its receptor for entry into the cell[32]. Since CD46, a regulator of the complement activation receptor, is expressed ubiquitously, HHV-6 can theoretically infect all human cell types including those of a germ cell lineage. Since spermatogenic cells undergo a considerably greater number of DNA replication and cell division events than any other cells, there may be a higher chance of an integration event due to telomere dysfunction, although germ cells do possess telomerase activity[33]. Our current findings that some identified CIHHV-6 cases have similar molecular characteristics suggest that integration is a rare event. We propose from this that a small number of ancestral chromosomes that had undergone a HHV-6 integration have likely expanded throughout the general human population as a neutral polymorphism.

Methods

Human subjects. We analyzed six Japanese cases that were suspected to CIHHV-6B by having genome-equivalent copy number of viral DNA in peripheral blood samples estimated by qPCR[20]. The clinical features of the cases are listed in Table 1. After informed consent was obtained, peripheral blood samples were obtained again from each patient for our genomic analyses. Our study was approved by the Ethical Review Board for Human Genome Studies at Fujita Health University (Accession number 90, approved on 24 March 2010). All cases provided their written informed consent to participate in this study.

Fluorescent in situ hybridization (FISH). FISH was performed using a standard method. Briefly, PHA-stimulated lymphocytes or EB-transformed lymphoblasts were arrested by treatment with colcemid. Metaphase preparations were obtained by hypotonic treatment using 0.075 M KCl followed by methanol/acetate fixation. A 10 kb PstI fragment of HHV-6 was used as the probe (Fig. 1a)[3,12]. Probes were labeled by nick-translation with biotin-16-dUTP or digoxigenin-11-dUTP. After hybridization, the probes were detected using either Alexa Fluor® 488-conjugated streptavidin or rhodamine-conjugated anti-digoxigenin, respectively. Chromosomes were visualized by counter-staining with 4′,6-diamino-2-phenylindole (DAPI). As reference standards, we used RP11-186O8 (22q11.21), TelVysion 6p SpectrumGreen and TelVysion Xq/Yq SpectrumOrange (Abbott Molecular, IllinoisI, USA).

Multiplex ligation-dependent probe amplification (MLPA). MLPA probe pairs were designed using a standard methodology[22] so that they are strategically distributed throughout the viral genome, the central unique long (UL) region and two DRs, as well as pac1 and pac2. In this strategy, MLPA probes consist of two oligonucleotides, each containing a PCR primer sequence and a variable length sequence complementary to the target. Genomic DNA was denatured (1 min at 98°C) and subsequently hybridized to the MLPA probe pairs in accordance with the manufacturer's protocol (MRC-Holland, Amsterdam, Netherlands). After ligation, probe pairs were amplified using universal primers. The multiplex PCR products were then separated on a capillary sequencer. For normalization, we created a plasmid harboring a tandem array of probe sequences separated by 10-nucleotide spacer and used this construct as a standard for the copy number. We only had an EB-transformed cell line for case 63 and did not use this sample for MLPA because the presence of the EB virus genome may affect the results.

Analysis of junction fragments. Southern hybridization was performed using a standard methodology. Briefly, genomic DNA was cleaved with appropriate restriction enzymes, followed by size-separation via 0.8% agarose gel electrophoresis. After denaturation, the DNA was blotted onto a nylon membrane. Probes were labeled by crosslinking with alkaline-phosphatase and detected using CDP-Star detection reagent (GE Healthcare, Buckinghamshire, UK). To isolate a junction fragment, standard or long-range PCR was performed using LA Taq (TaKaRa, Siga, Japan). The amplification conditions were 35 cycles of 10 sec at 98°C, 30 sec at 63°C and 10 min at 72°C. A PCR primer was designed using the sequence data for the human chromosome X genomic contig (accession number NT_167191.1) and that of the HST strain of HHV-6B (AB021506). X-2R primer: 5′-TTGTCTCAGGGTCCTAGTG-3′. The PCR products were sequenced using the Sanger method.

Mapping of the distal breakpoints. To map distal breakpoints on the viral genomes, long-range PCR was performed using LA Taq. PCR primers were designed using the sequence data for the HST strain of HHV-6B (AB021506). The amplification conditions were 35 cycles of 10 sec at 98°C, 30 sec at 63°C and 10 min at 72°C. For amplification of larger fragments, PCR cycles were increased up to 38 cycles. To amplify telomere repeats, we performed the PCR using the Tel-A primer, 5′-CCCTAACCCTAACCCTAACCCTAACC-3′. To show the smear products really contain telomeric repeats Southern hybridization was performed with a telomere-specific probe[34].

1. Abtashi, D. V. *et al.* Human herpesvirus-6 strain groups: a nomenclature. *Arch Virol* **129**, 363–366 (1993).
2. Dominguez, G. *et al.* Human herpesvirus 6B genome sequence: coding content and comparison with human herpesvirus 6A. *J Virol* **73**, 8040–8052 (1999).
3. Isegawa, Y. *et al.* Comparison of the complete DNA sequences of human herpesvirus 6 variants A and B. *J Virol* **73**, 8053–8063 (1999).
4. Yamanishi, K. *et al.* Identification of human herpesvirus-6 as a causal agent for exanthem subitum. *Lancet* **1**, 1065–1067 (1988).
5. Yoshikawa, T. *et al.* Distribution of antibodies to a causative agent of exanthem subitum (human herpesvirus-6) in healthy individuals. *Pediatrics* **84**, 675–677 (1989).
6. Fox, J. D., Briggs, M., Ward, P. A. & Tedder, R. S. Human herpesvirus 6 in salivary glands. *Lancet* **336**, 590–593 (1990).

7. Kondo, K., Kondo, T., Okuno, T., Takahashi, M. & Yamanishi, K. Latent human herpesvirus 6 infection of human monocytes/macrophages. *J Gen Virol* **72 (Pt 6)**, 1401–1408 (1991).
8. Yoshikawa, T. *et al.* Human herpesvirus-6 infection in bone marrow transplantation. *Blood* **78**, 1381–1384 (1991).
9. Yoshikawa, T. Human herpesvirus 6 infection in hematopoietic stem cell transplant patients. *Br J Haematol* **124**, 421–432 (2004).
10. Morissette, G. & Flamand, L. Herpesviruses and chromosomal integration. *J Virol* **84**, 12100–12109 (2010).
11. Hall, C. B. *et al.* Chromosomal integration of human herpesvirus 6 is the major mode of congenital human herpesvirus 6 infection. *Pediatrics* **122**, 513–520 (2008).
12. Tanaka-Taya, K. *et al.* Human herpesvirus 6 (HHV-6) is transmitted from parent to child in an integrated form and characterization of cases with chromosomally integrated HHV-6 DNA. *J Med Virol* **73**, 465–473 (2004).
13. Pellett, P. E. *et al.* Chromosomally integrated human herpesvirus 6: questions and answers. *Rev Med Virol* **22**, 144–155 (2011).
14. Nacheva, E. P. *et al.* Human herpesvirus 6 integrates within telomeric regions as evidenced by five different chromosomal sites. *J Med Virol* **80**, 1952–1958 (2008).
15. Thomson, B. J., Dewhurst, S. & Gray, D. Structure and heterogeneity of the a sequences of human herpesvirus 6 strain variants U1102 and Z29 and identification of human telomeric repeat sequences at the genomic termini. *J Virol* **68**, 3007–3014 (1994).
16. Gompels, U. A. & Macaulay, H. A. Characterization of human telomeric repeat sequences from human herpesvirus 6 and relationship to replication. *J Gen Virol* **76 (Pt 2)**, 451–458 (1995).
17. de Lange, T. How telomeres solve the end-protection problem. *Science* **326**, 948–952 (2009).
18. Arbuckle, J. H. *et al.* The latent human herpesvirus-6A genome specifically integrates in telomeres of human chromosomes in vivo and in vitro. *Proc Natl Acad Sci U S A* **107**, 5563–5568 (2010).
19. Arbuckle, J. H. & Medveczky, P. G. The molecular biology of human herpesvirus-6 latency and telomere integration. *Microbes Infect* **13**, 731–741 (2011).
20. Tanaka, N. *et al.* Monitoring four herpesviruses in unrelated cord blood transplantation. *Bone Marrow Transplant* **26**, 1193–1197 (2000).
21. Achour, A. *et al.* Length variability of telomeric repeat sequences of human herpesvirus 6 DNA. *J Virol Methods* **159**, 127–130 (2009).
22. Schouten, J. P. *et al.* Relative quantification of 40 nucleic acid sequences by multiplex ligation-dependent probe amplification. *Nucleic Acids Res* **30**, e57 (2002).
23. Celli, G. B., Denchi, E. L. & de Lange, T. Ku70 stimulates fusion of dysfunctional telomeres yet protects chromosome ends from homologous recombination. *Nat Cell Biol* **8**, 885–890 (2006).
24. Celli, G. B. & de Lange, T. DNA processing is not required for ATM-mediated telomere damage response after TRF2 deletion. *Nat Cell Biol* **7**, 712–718 (2005).
25. Arbuckle, J. H. *et al.* Mapping the telomere integrated genome of human herpesvirus 6A and 6B. *Virology* **442**, 3–11 (2013).
26. Flamand, L., Komaroff, A. L., Arbuckle, J. H., Medveczky, P. G. & Ablashi, D. V. Review, part 1: Human herpesvirus-6-basic biology, diagnostic testing, and antiviral efficacy. *J Med Virol* **82**, 1560–1568 (2010).
27. Leong, H. N. *et al.* The prevalence of chromosomally integrated human herpesvirus 6 genomes in the blood of UK blood donors. *J Med Virol* **79**, 45–51 (2007).
28. Wang, X. & Baumann, P. Chromosome fusions following telomere loss are mediated by single-strand annealing. *Mol Cell* **31**, 463–473 (2008).
29. Hall, C. B. *et al.* Congenital infections with human herpesvirus 6 (HHV6) and human herpesvirus 7 (HHV7). *J Pediatr* **145**, 472–477 (2004).
30. Feschotte, C. & Gilbert, C. Endogenous viruses: insights into viral evolution and impact on host biology. *Nat Rev Genet* **13**, 283–296 (2012).
31. Linardopoulou, E. V. *et al.* Human subtelomeres are hot spots of interchromosomal recombination and segmental duplication. *Nature* **437**, 94–100 (2005).
32. De Bolle, L., Naesens, L. & De Clercq, E. Update on human herpesvirus 6 biology, clinical features, and therapy. *Clin Microbiol Rev* **18**, 217–245 (2005).
33. Kurahashi, H. *et al.* Recent advance in our understanding of the molecular nature of chromosomal abnormalities. *J Hum Genet* **54**, 253–260 (2009).
34. Ijdo, J. W., Wells, R. A., Baldini, A. & Reeders, S. T. Improved telomere detection using a telomere repeat probe (TTAGGG)n generated by PCR. *Nucleic Acids Res* **19**, 4780 (1991).

Acknowledgments

The authors thank Dr. Hiroshi Kogo and Makiko Tsutsumi for helpful discussions, Akiko Yoshikawa, Noriko Hayashizono and Narumi Kamiya for technical assistance. This work was supported by a grant-in-aid for Scientific Research from the Ministry of Education, Culture, Sports, Science, and Technology of Japan (24390085, 23659182, 23013019, http://www.mext.go.jp), and from the Ministry of Health, Labour and Welfare of Japan, to H.K (10103465, http://www.mhlw.go.jp).

Author contributions

T.O., T.Y. and H.K. conceived and designed the experiments. T.O. performed all the experiments. I.H., M.I., Y.H., K.K., J.O., H.Y., T.N., Y.T., S.K. and T.Y., contributed regents and materials. T.O. and H.K. wrote the manuscript. All authors reviewed the manuscript.

Additional information

Supplementary information accompanies this paper at http://www.nature.com/scientificreports

Competing financial interests: The authors declare no competing financial interests.

How to cite this article: Ohye, T. *et al.* Dual roles for the telomeric repeats in chromosomally integrated human herpesvirus-6. *Sci. Rep.* **4**, 4559; DOI:10.1038/srep04559 (2014).

Accurate Prediction of the Stage of Histological Chorioamnionitis before Delivery by Amniotic Fluid IL-8 Level

Satoshi Yoneda[1], Arihiro Shiozaki[1], Mika Ito[1], Noriko Yoneda[1], Kumiko Inada[1], Rika Yonezawa[1], Mika Kigawa[2], Shigeru Saito[1]

[1]Department of Obstetrics and Gynecology, University of Toyama, Toyama, Japan;
[2]Department of Public Health Faculty of Medicine, University of Toyama, Toyama, Japan

Keywords
Amniotic fluid, body temperature, histological chorioamnionitis, interleukin-8, preterm labor

Correspondence
Shigeru Saito, Department of Obstetrics and Gynecology, University of Toyama, 2630 Sugitani, Toyama, 930-0194, Japan.
E-mail: s30saito@med.u-toyama.ac.jp

Submission December 4, 2014;
accepted January 2, 2015.

Citation
Yoneda S, Shiozaki A, Ito M, Yoneda N, Inada K, Yonezawa R, Kigawa M, Saito S. Accurate prediction of the stage of histological chorioamnionitis before delivery by amniotic fluid IL-8 level. Am J Reprod Immunol 2015

doi:10.1111/aji.12360

Objective
To estimate the stage of histological chorioamnionitis (h-CAM) antenatally using clinical data.

Materials and methods
Four hundred and twenty-eight singleton mothers were recruited. Clinical data including the levels of white blood cell count (WBC), C-reactive protein (CRP), amniotic fluid interleukin-8 (AF-IL-8) at Cesarean section, and maternal body temperature (MBT) were collected.

Results
Histological chorioamnionitis was present in 45.3% of the cases. Poor neonatal prognosis was highest (59.1%) in cases with h-CAM stage III. AF-IL-8 (odds ratio: 8.5, 95% CI: 5.1-14.8, $P < 0.0001$) and MBT (odds ratio: 2.3, 95% CI: 1.13–4.1, $P = 0.0192$) were independent risk factors for h-CAM. The cutoff value of AF-IL-8 for predicting each stage of h-CAM (stage I or higher, stage II or higher, and stage III) were ≥9.9 ng/mL, ≥17.3 ng/mL, and ≥55.9 ng/mL, respectively.

Conclusion
The stage of h-CAM was able to be predicted accurately by the level of AF-IL-8 before delivery.

Introduction

Histological chorioamnionitis (h-CAM) is an antenatal inflammatory state of the intrauterine environment strongly associated with preterm delivery. Around 33–83% of infants born before 30–32 weeks of gestation have been exposed to h-CAM,[1–5] which often is a clinically silent process. Exposure to h-CAM is known to induce several organ failures in the fetus.[6] Its presence in placentas from preterm infants increases the incidence of bronchopulmonary dysplasia (BPD),[7–9] necrotizing enterocolitis (NEC),[2,10] periventricular leukomalacia (PVL),[11,12] and cerebral palsy (CP).[12–17] These are recognized as symptoms of fetal response inflammatory syndrome (FIRS).[18–20] These effects have been generally shown to be more pronounced when additional signs of fetal inflammation, such as funisitis, are present.[21–24]

Histological chorioamnionitis is classified into three stages according to Blanc's classification: stage I (deciduitis), stage II (chorionitis), and stage III (amnionitis).[25] van Hoeven et al.[26] reported that the risk of FIRS becomes higher with an increase in the severity of h-CAM. However, the associations between h-CAM and inflammatory markers in maternal circulation have not been fully clarified. On the other hand, clinical CAM was defined by Lenki et al.[27] as maternal fever (≥38.0°C), elevated white blood cell count (≥15,000/μL), uterine tenderness, maternal or fetal tachycardia, and malodorous

vaginal fluid. Although clinical CAM may be clearly diagnosed before delivery, neonatal outcomes may already be deteriorated by that point in time,[14,28,29] suggesting that clinical CAM is a final stage of CAM. Park et al.[30] reported that the involvement of the amnion in the inflammatory process of the extraplacental membranes is associated with a more intense fetal inflammatory response than chorionitis alone. Therefore, an accurate prediction of h-CAM and its degree are needed to manage mothers with pre-clinical symptoms of clinical CAM before the appearance of clinical symptoms.

To overcome this problem, the ability of biological markers to detect h-CAM before birth has been investigated. There have been some reports evaluating h-CAM during pregnancy by biological markers, such as maternal body temperature (MBT),[27,31] maternal white blood cell count (WBC),[27,31] maternal C-reactive protein (CRP),[30,32,33] maternal or amniotic interleukin (IL)-6,[34–37] and amniotic IL-8.[38] However, there have been no reports predicting antenatally the severity of h-CAM by biological and clinical markers.

Information about the severity of h-CAM during the antenatal preterm period may be clinically useful for the management of cases at risk for preterm labor or with cervical incompetency. Additionally, with detection of strong intrauterine inflammation before clinical CAM, early termination of the pregnancy may be considered. On the other hand, no detection of inflammation or weak inflammation in the uterus would allow an extended period of pregnancy by maintenance tocolysis. Therefore, the degree of uterine inflammation should be evaluated before delivery, and individual strategies to improve neonatal prognosis for each case should be developed even if there is no sign of clinical CAM.

This study is the first report to show that amniotic fluid IL-8 levels are a good marker for estimating the stage of h-CAM in the antenatal period.

Materials and methods

Study Population

Four hundred and twenty-eight mothers who underwent Cesarean sections were recruited at Toyama University Hospital between January 2009 and December 2013. Two hundred and fifteen cases delivered preterm babies and 213 cases full-term babies. We excluded cases with premature rupture of membranes (PROM), preterm birth within 2 days of maternal steroid treatment leading to increased maternal WBC, severe fetal growth retardation (less than −2.0 S.D.), severe congenital abnormalities, polyhydramnios, gestational diabetes mellitus, preeclampsia, multiple pregnancies, and Cesarean sections due to failure of vaginal trial labor. The study was approved by the ethics committee of Toyama University Hospital. All the subjects included in this study provided informed written consent.

Definitions and Study Procedures

Gestational age was determined from the first day of the last menstrual period, or by fetal size by transvaginal ultrasound before 12 weeks of gestation.

The stages of h-CAM are defined by the degree of the neutrophil infiltration to the amnion–chorion–decidua. The stage I is defined that maternal neutrophils are between the decidua and chorionic plate. The stage II is defined that maternal neutrophils are in the connective tissues of the chorionic plate. Stage III is characterized by neutrophil infiltration of the amnion according to Blanc's diagnostic criteria.[25] And the funisitis was defined as the presence of any vasculitis in the umbilical cord. Section of tissue blocks were stained with hematoxylin–eosin and examined systematically for inflammation by some pathologists unaware of the proteomic results of the amniotic fluid in their laboratory rooms.

Demographic and clinical data (maternal data included age, parity, gestational age at delivery, intrapartum fever, and mode of delivery) were collected. Clinical CAM was defined as the combination of maternal fever during labor (more than 38°C) with any one of the following: maternal tachycardia (≥100 beats/min), uterine tenderness, malodorous amniotic fluid, or maternal leukocytosis (≥15,000 white blood cells/mL).

Poor neonatal outcome was defined as neonatal death or diagnosis of periventricular leukomalacia (PVL), intraventricular hemorrhage (IVH) ≥grade III, bronchopulmonary dysplasia (BPD), and necrotizing enterocolitis (NEC) during hospitalization in the NICU. PVL was defined by de Vries,[39] the classification of IVH was defined by Papile et al.[40] moderate/severe BPD was defined as an oxygen requirement at 36 weeks of gestational age according to the NICHD consensus conference paper,[41] and NEC was defined according to modified Bell's criteria[42] with ≥stage II considered to be significant.

Sample Collection and Preparation

Maternal body temperature was measured just before Cesarean section. In preterm delivery, blood tests (maternal WBC and CRP) were performed within 48 hr before Cesarean section. In the case of elective Cesarean section, which was usually planned at about 39 weeks of gestation in full-term delivery, the blood test was performed within 2 weeks before the Cesarean section. However, in cases with high maternal fever before elective Cesarean section, levels of WBC and CRP were examined again just prior to Cesarean section. Amniotic fluid was extracted directly from the amniotic cavity just before delivery.

Management of Preterm Labor

When the patients are diagnosed as preterm labor, they are immediately hospitalized for bed rest and recommended the treatment of maintenance tocolysis (continuous intravenous infusion of ritodrine hydrochloride or magnesium sulfate) until 36 weeks of gestation to prevent the preterm birth.[43,44] During the long hospitalization, the clinical symptom would go on severer such as bag formation in the cervix, maternal WBC >15,000/μL, or maternal CRP >1.0 mg/dL; intravenous antibiotics (beta-lactam antibiotics 2–3 g/day or EM 800–1500 mg/day for 7 days) are empirically considered by obstetricians. Therefore, we could often use the antibiotics for preterm labor in long hospitalization.

Detection of AF-IL-8

The IL-8 is a chemokine produced by a variety of cell types, and various diseases related as a pro-inflammatory marker were reported.[45–47] We considered that it was a very good marker for the early stage of inflammation in the amnion, and routinely measured amniotic IL-8 level since 2001. In our previous study, amniotic IL-8 level was most reflected at each stage of h-CAM among the level of amniotic IL-8, TNFα, and IL-17.[48]

About 10 mL of amniotic fluid was obtained before delivery. AF-IL-8 was measured by an enzyme-linked immunosorbent assay (ELISA) as previously reported.[49] The detection limit of AF-IL-8 by ELISA was 32 pg/mL. On average, intra-assay and interassay coefficients of variation were 4.8% and 7.5%, respectively. The remaining sample of the amniotic fluid was stored at −80°C.

Statistical Analysis

To identify relevant clinical variables that varied between the h-CAM-positive and h-CAM-negative groups, univariate analysis was performed using the χ^2 test, Student's *t*-test, or Mann–Whitney *U*-test where appropriate. The association between the severity of h-CAM and lower gestational age at delivery was analyzed by ANOVA, and the risk factor of poor neonatal outcome was evaluated by logistic regression analysis. A cutoff value to predict h-CAM was proposed by receiver-operating characteristic (ROC) curves, and logistic regression analysis was performed to investigate the most reliable biochemical marker for the prediction of h-CAM. Odds ratios and 95% confidence intervals (95% CI) were also calculated. Diagnostic values of sensitivity, specificity, positive predictive value (PPV), and negative predictive value (NPV) were estimated to predict h-CAM. The cutoff values to predict the stage of h-CAM were determined using the most reliable biochemical marker. All analyses were performed using statistical analysis software (JMP 9.02; SAS Institute Inc, Tokyo, Japan). A *P* value of below 0.05 was regarded as significant.

Results

The patient characteristics of this study are shown in Table I. There were 215 (50.2%) cases of preterm delivery and 213 (49.8%) cases of full-term delivery. The frequency of stage I, stage II, and stage III h-CAM was 47.4, 35.0, and 17.6%, respectively. Clinical CAM was only detected in h-CAM(+) cases, with the frequency being very low (1.0%). Preterm birth was more frequent, and the gestational age was shorter in h-CAM-positive cases compared to h-CAM-negative cases. Funisitis was observed in 32.5% of h-CAM-positive cases, while it was observed in only 0.8% of h-CAM-negative cases.

There was a significant association between the severity of h-CAM and lower gestational age at delivery (ANOVA; $P < 0.0001$), and the incidence of poor neonatal outcome, such as neonatal death ($n = 4$), PVL ($n = 4$), IVH ≥grade III ($n = 2$), BPD ($n = 11$), and NEC ($n = 1$), was highest (59.1%) in stage III h-CAM (Fig. 1). The severity of h-CAM (odds ratio: 2.7, 95%CI: 1.6–5.0, $P = 0.0004$) and

Table I Characteristics of Patients (N = 428)

	h-CAM (–) (N = 234)	h-CAM (+) (N = 194)	P
Maternal age (year)	33 (18–43)	33 (20–44)	0.3036
Nulliparity (%)	35.9 (84/234)	40.2 (78/194)	0.3602
Antibiotic therapy (%)	6.4 (15/234)	29.9 (58/194)	<0.0001
Preterm birth (%)	41.4 (97/234)	60.8 (118/194)	0.0001
Delivery (w)	37 (24–41)	33 (24–41)	<0.0001
c-CAM (%)	0 (0/234)	1.0 (2/194)	–
Funisitis (%)	0.8 (2/234)	32.5 (63/194)	<0.0001
h-CAM stage I (%)		47.4 (92/194)	–
h-CAM stage II (%)		35.0 (68/194)	–
h-CAM stage III (%)		17.6 (34/194)	–

c-CAM, clinical chorioamnionitis; h-CAM, histological chorioamnionitis.

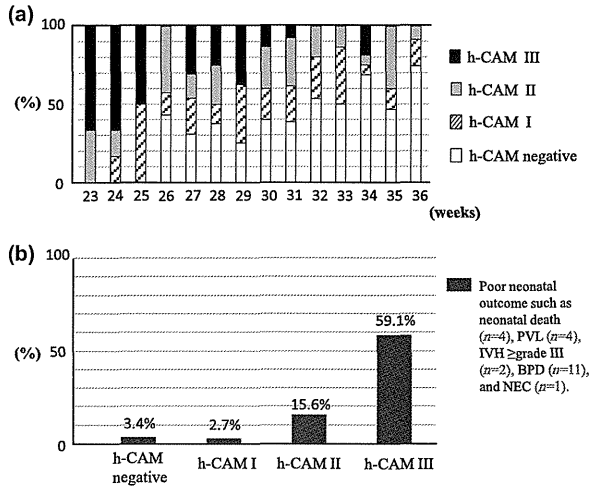

Fig. 1 The ratio of the stage of histological chorioamnionitis (h-CAM) to gestational age at delivery. There was a significant relationship between the severity of h-CAM and lower gestational age at delivery. (ANOVA; $P < 0.0001$) (a) Ratio of poor neonatal prognosis including neonatal death, PVL, IVH ≥stage III, BPD, and NEC. Cases of h-CAM stage III have the highest incidence of poor neonatal prognosis (59.1%) (b).

lower gestational age at delivery (odds ratio: 1.3/week, 95%CI: 1.1–1.6, $P = 0.0009$) were independent risk factors of poor neonatal outcome.

Table II shows the averages of four markers (MBT, WBC, CRP, and AF-IL-8) in h-CAM-positive and h-CAM-negative cases. MBT [36.8 (35.1–38.8)°C], WBC [8520 (4500–23,880)/μL], CRP [0.24 (0.02–9.9) mg/dL], and AF-IL-8 [19.7 (0.1–566.5) ng/mL] were significantly higher in h-CAM-positive cases than in h-CAM-negative cases [36.7 (35.0–37.6)°C, 7600 (2490–22,940)/μL, 0.20 (0.02–4.8) mg/dL, and 2.9 (0.1–162.6) ng/mL] ($P < 0.0001$, $P = 0.0002$, $P = 0.0006$, and $P < 0.0001$, respectively). The cutoff values to predict h-CAM were ≥9.9 ng/mL (AF-IL-8), ≥9800/μL (WBC), ≥0.44 mg/dL (CRP), and ≥37.1°C (MBT), respectively (Fig. 2). The area under curve (AUC) of AF-IL-8 (AUC = 0.7653) was significantly larger than those of WBC (AUC = 0.6070), CRP (AUC = 0.5970), and MBT (AUC = 0.6251), respectively ($P < 0.0001$, each) (Fig. 2).

AF-IL-8 (odds ratio: 8.5, 95% CI: 5.1–14.8, $P < 0.0001$) and MBT (odds ratio: 2.3, 95% CI:

Table II Clinical Data in Cases With or Without Histological Chorioamnionitis

	h-CAM (–) (N = 234)	h-CAM (+) (N = 194)	P
MBT (°C)	36.7 (35.0–37.6)	36.8 (35.1–38.8)	<0.0001
WBC (/μL)	7600 (2490–22,940)	8520 (4500–23,880)	0.0002
CRP (mg/dL)	0.20 (0.02–4.8)	0.24 (0.02–9.9)	0.0006
AF-IL-8 (ng/mL)	2.9 (0.1–162.6)	19.7 (0.1–566.5)	<0.0001

h-CAM, histological chorioamnionitis; MBT, maternal body temperature; WBC, white blood cell; CRP, C-reactive protein; AF-IL-8, amniotic fluid interleukin-8.

American Journal of Reproductive Immunology (2015)

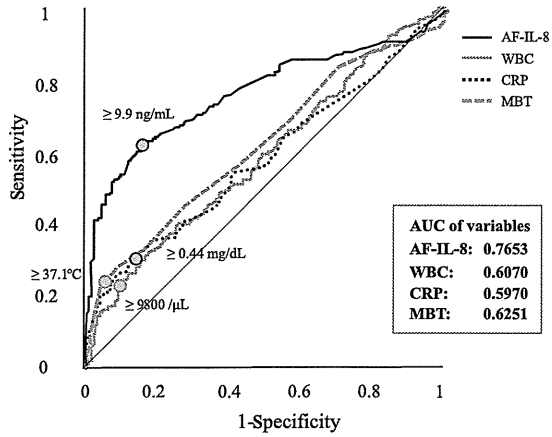

Fig. 2 Receiver-operating curves for amniotic fluid IL-8 (area under curve = 0.7653, $P < 0.0001$ for each AUC of maternal BT, CRP, WBC) for the prediction of histological chorioamnionitis.

1.13–4.1, $P = 0.0192$) were independent risk factors for h-CAM among the four markers (Table III). The level of AF-IL-8 predicted h-CAM with a sensitivity of 57.7%, a specificity of 88.9%, a PPV of 81.1%, and a NPV of 71.7%, while MBT predicted h-CAM with a sensitivity of 27.8%, a specificity of 91.4%, a PPV of 73.0%, and a NPV of 60.4% (Table IV).

Using the level of AF-IL-8, the cutoff value was evaluated to predict the stage of h-CAM before delivery. The cutoff values for h-CAM of stage I or higher, stage II or higher, and stage III were ≥9.9, ≥17.3, and ≥ 55.9 ng/mL, respectively (Fig. 3). The sensitivities for predicting h-CAM of stage I or higher, stage II or higher, and stage III were 57.7, 77.4, and 91.2%, with specificities of 88.9, 85.3, and 91.4%, respectively (Table V).

Although the frequency of funisitis was significantly increased with increase in the stage of h-CAM (Table VI), AF-IL-8 levels in each stage of h-CAM with or without funisitis were similar (Table VII).

Table III Logistic Regression Analysis for the Prediction of Histological Chorioamnionitis

	Odds ratio	95% CI	*P*
MBT (>37.1°C)	2.3	1.13–4.1	0.0192
WBC (>9800/μL)	1.1	0.62–1.9	0.7204
CRP (>0.44 mg/dL)	1.3	0.77–2.3	0.2986
AF-IL-8 (>9.9 ng/mL)	8.5	5.1–14.8	<0.0001

CI, confidence interval; MBT, maternal body temperature; WBG, white blood cell; CRP, C-reactive protein; AF-IL-8, amniotic fluid interleukin-8.

Discussion

Strengths and Weakness of the Study

The following are major strengths of this study. (i) This study was comprised of a large cohort of women with singleton babies ($N = 428$) and with histologic chorioamnionitis ($N = 194$). (ii) We evaluated several markers of infection and inflammation including AF-IL-8, MBT, WBC, and CRP. We found both AF-IL-8 and MBT were independent markers to predict h-CAM before delivery, and the predictive value for h-CAM was higher in AF-IL-8 compared to MBT. (iii) We have shown for the first time that the level of AF-IL-8 was able to estimate the stage of h-CAM before delivery. The cutoff value of AF-IL-8 to predict stage I or higher was ≥9.9 ng/mL with a sensitivity of 57.7% and a specificity of 88.9%. The cutoff value to predict stage II or higher was ≥17.3 ng/mL with a sensitivity of 77.4% and a specificity of 85.3%. The cutoff value to predict stage III of h-CAM was ≥55.9 ng/mL with a sensitivity of 91.2% and a specificity of 91.4%. (iv) In our study, poor neonatal prognosis, such as neonatal death, PVL, IVH ≥grade III, BPD, and NEC, was extremely high in cases of stage III h-CAM. When h-CAM stage III is estimated by AF-IL-8 level, termination of pregnancy may be considered. However, the gestational age at that point in time must also be considered for fetal prematurity.

Table IV Diagnostic Factors for the Prediction of Histological Chorioamnionitis

	Sensitivity (%)	Specificity (%)	PPV (%)	NPV (%)
AF-IL-8 (>9.9 ng/mL)	57.7 (112/194)	88.9 (208/234)	81.1 (112/138)	71.7 (208/290)
MBT (>37.1°C)	27.8 (54/194)	91.4 (214/234)	73.0 (54/74)	60.4 (214/354)

AF-IL-8, amniotic fluid interleukin-8; MBT, maternal body temperature; PPV, positive predictive value; NPV, negative predictive value.

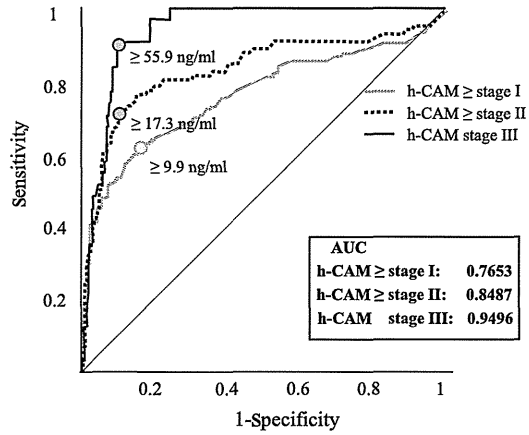

Fig. 3 Cutoff values of amniotic fluid IL-8 to predict the stages of histological chorioamnionitis. The area under curve for the prediction of histological chorioamnionitis stage I or higher, stage II or higher, and stage III is 0.7653, 0.8487, and 0.9496, respectively.

Table VI Frequency of Funisitis in Each Stage of Histological Chorioamnionitis

h-CAM	Frequency of funisitis		
Stage I	8.7 (8/92)	$P < 0.0001$	$P < 0.0001$
Stage II	43.9 (29/68)	$P = 0.0012$	
Stage III	76.5 (26/34)		

h-CAM, histological chorioamnionitis.

Table VII Association between Amniotic Fluid IL-8 and Funisitis in Each Stage of Histological Chorioamnionitis

	Funisitis (+)	Funisitis (−)	*P*
AF-IL-8 (ng/mL)			
Stage I	12.5 (0.1–40.2)	5.8 (0.1–240.6)	0.4142
Stage II	21.2 (0.1–379.5)	39.6 (0.1–376.7)	0.6944
Stage III	165.6 (17.5–566.5)	118.7 (26.5–237.5)	0.1679

h-CAM, histological chorioamnionitis; AF-IL-8, amniotic fluid interleukin-8.

The following are potential weaknesses of this study. (i) While in most cases WBC and CRP were examined just prior to Cesarean section, some full-term delivery cases without symptoms were examined within 2 weeks. (ii) We report no information about the levels of other cytokines in the amniotic fluid. Amniotic IL-8 level was measured because it has been reported that amniotic fluid IL-8 levels gradually increased with the h-CAM stage.[48] Amniotic TNF-α and IL-17 levels are only elevated in stage III of h-CAM.[48] Holst et al.[50] reported that among 27 proteins in the amnion, amniotic macrophage protein-1β (MIP-1β) is useful to predict delivery within 7 days. Keeler et al.[51] also reported that among 25 amniotic cytokines, monocyte chemotactic protein-1 (MCP-1) is the best marker for the prediction of early delivery. Using these suggested amniotic markers reflecting strong inflammation in the amnion, further detail of h-CAM may be able to be provided. Further studies are needed to clarify which cytokines are the best suited to evaluate the stage of h-CAM. (iii) When the stage III of h-CAM will be predicted by amniotic IL-8 levels, certainly, the best treatment was not leaded in this study. However, using this result of predicting the accurate stage of h-CAM antenatally, the new strategy might be effective to prevent the neonatal outcomes in the future studies.

Clinical Significance of this Study

Lenki et al.[27] reported that clinical CAM may be diagnosed by symptoms and blood examination, although the prognosis of the neonate is usually poor by the time clinical CAM is made evident.[10,28] This study reported a very low frequency of clinical CAM, suggesting that the majority of the h-CAM cases were terminated before the onset of clinical CAM. This evidence prompted us to establish a new

Table V Diagnostic Factors for the Prediction of Histological Chorioamnionitis Stages

	Sensitivity (%)	Specificity (%)	PPV (%)	NPV (%)
h-CAM > stage I (>9.9 ng/mL)	57.7 (112/194)	88.9 (208/234)	81.1 (112/138)	71.7 (208/290)
h-CAM > stage II (>17.3 ng/mL)	77.4 (79/102)	85.3 (278/326)	62.2 (79/127)	92.3 (278/301)
h-CAM stage III (>55.9 ng/mL)	91.2 (31/34)	91.4 (360/394)	47.7 (31/65)	99.2 (360/363)

h-CAM, histological chorioamnionitis; PPV, positive predictive value; NPV, negative predictive value.

strategy for diagnosing h-CAM before the appearance of clinical signs. Therefore, recognition of h-CAM as a pre-stage of clinical chorioamnionitis may allow better management of women at risk for preterm labor or cervical incompetency and avoid poor neonatal prognosis such as neonatal death, PVL, IVH ≥grade III, BPD, and NEC.

An accurate prediction of the stage of h-CAM is important to provide proper treatment. Compared to cases with h-CAM, pregnancies without h-CAM should be extended as long as possible. Although there has been no evidence showing the efficacy of maintenance tocolysis for treatment, it may be effective for treatment of low-grade h-CAM predicted antenatally. Knowing the estimated grade of h-CAM, we may be able to determine an appropriate time for delivery in cases of severe intrauterine inflammation to avoid a poor outcome for the baby. We have reported that clinical symptoms and AF-IL-8 may be used to estimate the time of delivery in preterm labor cases.[52]

The aim of this study was only to lead the cutoff value of amniotic IL-8 levels to predict each stage of h-CAM by using large number of amniotic samples. Therefore, the sample included cases of the third trimester. The evaluation of amniocentesis to predict the stage of h-CAM was clinically for less than 30 weeks of gestation.

The Correlation between AF-IL-8 and Funisitis

It was reported that the risk of FIRS increases with the presence of h-CAM. The severity of h-CAM influences FIRS, although the degree of influence on the fetus is unknown. Funisitis can also increase the risk of FIRS.[21–24] In the present study, there was no correlation between the level of AF-IL-8 and funisitis in any of the stages of h-CAM (Table VI). The level of AF-IL-8 was strongly correlated with the stage of h-CAM, irrespective of the existence of funisitis. These data suggested that AF-IL-8 is a good marker for h-CAM, but not for predicting funisitis.

Questions in this Study

The antibiotic therapy has the effect just to microbes, not inflammation. And the preterm delivery was strongly correlated with amniotic inflammation (h-CAM) rather than the microbes in the amnion.[53,54] Therefore, antibiotic therapy was considered not to influence the amniotic fluid IL-8 levels.

Despite the high rate of preterm birth of 41% in h-CAM-negative group, the rate of delivery before 33 weeks of gestation was 14.9% (35/234) without h-CAM, while 38.6% (75/194) with h-CAM. The rate of preterm delivery of 41% was certainly high; however, most cases were delivered after 33 weeks of gestation without h-CAM.

The frequency of clinical CAM was only 1%: The reason was considered that (i) in this study, we excluded the premature rupture of the membranes (PROM) that often happened to clinical CAM. (ii) A large numbers of sample cases after 33 weeks of gestations were included in our study (73.8%).

Unanswered Questions and Proposals for Future Research

At present, the stage of h-CAM cannot predict the condition of the baby before delivery. Therefore, a prediction of the stage of h-CAM as part of the management of cases at risk for preterm labor or cervical incompetency may improve the prognosis of neonates. Maintenance tocolysis may be performed in cases without h-CAM or with h-CAM stage I, while a short-term tocolysis may be carried out in cases with h-CAM stage II or III. In cases with h-CAM stage III and with a positive microbubble test showing fetal lung maturation, delivery of the baby should be considered as an option, taking into account the gestational age. In conclusion, the stage of h-CAM may be predicted accurately by the level of AF-IL-8 before delivery.

References

1 Lahra MM, Jeffery HE: A fetal response to chorioamnionitis is associated with early survival after preterm birth. *Am J Obstet Gynecol* 2004; 190:147–151.
2 Been JV, Rours IG, Kornelisse RF, Lima Passos V, Kramer BW, Schneider TA, de Krijger RR, Zimmermann LJ: Histologic chorioamnionitis, fetal involvement, and antenatal steroids: effects on neonatal outcome in preterm infants. *Am J Obstet Gynecol* 2009; 201:587. e581–588.
3 Been JV, Zimmermann LJ: Histological chorioamnionitis and respiratory outcome in preterm infants. *Arch Dis Child Fetal Neonatal Ed* 2009; 94:F218–F225.
4 Erdemir G, Kultursay N, Calkavur S, Zekioğlu O, Koroglu OA, Cakmak B, Yalaz M, Akisu M, Sagol S: Histological chorioamnionitis: effects on premature delivery and neonatal prognosis. *Pediatr Neonatol* 2013; 54:267–274.
5 Ogunyemi D, Murillo M, Jackson U, Hunter N, Alperson B: The relationship between placental histopathology findings and

perinatal outcome in preterm infants. *J Matern Fetal Neonatal Med* 2003; 13:102–109.
6 Gantert M, Been JV, Gavilanes AW, Garnier Y, Zimmermann LJ, Kramer BW: Chorioamnionitis: a multiorgan disease of the fetus? *J Perinatol* 2010; 30:S21–S30.
7 Kotecha S: Cytokines in chronic lung disease of prematurity. *Eur J Pediatr* 1996; 155:S14–S17.
8 Speer CP: Inflammatory mechanisms in neonatal chronic lung disease. *Eur J Pediatr* 1999; 158:S18–S22.
9 Zanardo V, Vedovato S, Trevisanuto DD, Suppiej A, Cosmi E, Fais GF, Chiarelli S: Histological chorioamnionitis and neonatal leukemoid reaction in low-birth-weight infants. *Hum Pathol* 2006; 37:87–91.
10 Been JV, Lievense S, Zimmermann LJ, Kramer BW, Wolfs TG: Chorioamnionitis as a Risk Factor for Necrotizing Enterocolitis: a Systematic Review and Meta-Analysis. *J Pediatr* 2013; 162:236–242. e2.
11 Yoon BH, Romero R, Yang SH, Jun JK, Kim IO, Choi JH, Syn HC: Interleukin-6 concentrations in umbilical cord plasma are elevated in neonates with white matter lesions associated with periventricular leukomalacia. *Am J Obstet Gynecol* 1996; 174:1433–1440.
12 Wu YW, Colford JM Jr: Chorioamnionitis as a risk factor for cerebral palsy: a meta-analysis. *JAMA* 2000; 284:1417–1424.
13 Bashiri A, Burstein E, Mazor M: Cerebral palsy and fetal inflammatory response syndrome: a review. *J Perinat Med* 2006; 34:5–12.
14 Yoon BH, Park CW, Chaiworapongsa T: Intrauterine infection and the development of cerebral palsy. *BJOG* 2003; 110:124–127.
15 Yoon BH, Romero R, Park JS, Kim CJ, Kim SH, Choi JH, Han TR: Fetal exposure to an intra-amniotic inflammation and the development of cerebral palsy at the age of three years. *Am J Obstet Gynecol* 2000; 182:675–681.
16 Soraisham AS, Trevenen C, Wood S, Singhal N, Sauve R: Histological chorioamnionitis and neurodevelopmental outcome in preterm infants. *J Perinatol* 2013; 33:70–75.
17 Shatrov JG, Birch SC, Lam LT, Quinlivan JA, McIntyre S, Mendz GL: Chorioamnionitis and cerebral palsy: a meta-analysis. *Obstet Gynecol* 2010; 116:387–392.
18 Hofer N, Kothari R, Morris N, Müller W, Resch B: The fetal inflammatory response syndrome is a risk factor for morbidity in preterm neonates. *Am J Obstet Gynecol* 2013; 209:542. e1-542.e11.
19 Gomez R, Romero R, Ghezzi F, Yoon BH, Mazor M, Berry SM: The fetal inflammatory response syndrome. *Am J Obstet Gynecol* 1998; 179:194–202.
20 Gotsch F, Romero R, Kusanovic JP, Mazaki-Tovi S, Pineles BL, Erez O, Espinoza J, Hassan SS: The fetal inflammatory response syndrome. *Clin Obstet Gynecol* 2007; 50:652–683.
21 Lahra MM, Beeby PJ, Jeffery HE: Maternal versus fetal inflammation and respiratory distress syndrome: a 10-year hospital cohort study. *Arch Dis Child Fetal Neonatal Ed* 2009; 94:F13–F16.
22 D'Alquen D, Kramer BW, Seidenspinner S, Marx A, Berg D, Groneck P, Speer CP: Activation of umbilical cord endothelial cells and fetal inflammatory response in preterm infants with chorioamnionitis and funisitis. *Pediatr Res* 2005; 57:263–269.
23 Pacora P, Chaiworapongsa T, Maymon E, Kim YM, Gomez R, Yoon BH, Ghezzi F, Berry SM, Qureshi F, Jacques SM, Kim JC, Kadar N, Romero R: Funisitis and chorionic vasculitis: the histological counterpart of the fetal inflammatory response syndrome. *J Matern Fetal Neonatal Med* 2002; 11:18–25.
24 Kim CJ, Yoon BH, Park SS, Kim MH, Chi JG: Acute funisitis of preterm but not term placentas is associated with severe fetal inflammatory response. *Hum Pathol* 2001; 32:623–629.
25 Blanc WA: Pathology of the placenta, membranes and umbilical cord in bacterial, fungal, and viral infections in man. *In* Perinatal Disease, RL Naeye (ed). Baltimore, Williams & Wilkins, 1981, pp 67–132.
26 van Hoeven KH, Anyaegbunam A, Hochster H, Whitty JE, Distant J, Crawford C, Factor SM: Clinical significance of increasing histologic severity of acute inflammation in the fetal membranes and umbilical cord. *Pediat Pathol Lab Med* 1996; 16:731–744.
27 Lenki SG, Maciulla MB, Eglinton GS: Maternal and umbilical cord serum interleukin level in preterm labor with clinical chorioamnionitis. *Am J Obstet Gynecol* 1994; 170:1345–1351.
28 Lieberman E, Lang J, Richardson DK, Frigoletto FD, Heffner LJ, Cohen A: Intrapartum maternal fever and neonatal outcome. *Pediatrics* 2000; 105:8–13.
29 Nasef N, Shabaan AE, Schurr P, Iaboni D, Choudhury J, Church P, Dunn MS: Effect of clinical and histological chorioamnionitis on the outcome of preterm infants. *Am J Perinatol* 2013; 30:59–68.
30 Park CW, Moon KC, Park JS, Jun JK, Romero R, Yoon BH: The involvement of human amnion in histologic chorioamnionitis is an indicator that a fetal and an intra-amniotic inflammatory response is more likely and severe: clinical implications. *Placenta* 2009; 30:56–61.
31 Roberts DJ, Celi AC, Riley LE, Onderdonk AB, Boyd TK, Johnson LC, Lieberman E: Acute histologic chorioamnionitis at term: nearly always noninfectious. *PLoS ONE* 2012; 7:e31819.
32 van de Laar R, van der Ham DP, Oei SG, Willekes C, Weiner CP, Mol BW: Accuracy of C-reactive protein determination in predicting chorioamnionitis and neonatal infection in pregnant women with premature rupture of membranes: a systematic review. *Eur J Obstet Gynecol Reprod Biol* 2009; 147:124–129.
33 Trochez-Martinez RD, Smith P, Lamont RF: Use of C-reactive protein as a predictor of chorioamnionitis in preterm prelabour rupture of membranes: a systematic review. *BJOG* 2007; 114:796–801.
34 Maeda K, Matsuzaki N, Fuke S, Mitsuda N, Shimoya K, Nakayama M, Suehara N, Aono T: Value of the maternal interleukin 6 level for determination of histologic chorioamnionitis in preterm delivery. *Gynecol Obstet Invest* 1997; 43:225–231.
35 Gulati S, Bhatnagar S, Raghunandan C, Bhattacharjee J: Interleukin-6 as a predictor of subclinical chorioamnionitis in preterm premature rupture of membranes. *Am J Reprod Immunol* 2012; 67:235–240.
36 Kacerovsky M, Musilova I, Hornychova H, Kutova R, Pliskova L, Kostal M, Jacobsson B: Bedside assessment of amniotic fluid interleukin-6 in preterm prelabor rupture of membranes. *Am J Obstet Gynecol* 2014; 211:385. e1-9.
37 Cobo T, Kacerovsky M, Palacio M, Hornychova H, Hougaard DM, Skogstrand K, Jacobsson B: A prediction model of histological chorioamnionitis and funisitis in preterm prelabor rupture of membranes: analyses of multiple proteins in the amniotic fluid. *J Matern Fetal Neonatal Med* 2012; 25:1995–2001.
38 Kacerovsky M, Drahosova M, Hornychova H, Pliskova L, Bolehovska R, Forstl M, Tosner J, Andrys C: Value of amniotic fluid interleukin-8 for the prediction of histological chorioamnionitis in preterm premature rupture of membranes. *Neuro Endocrinol Lett* 2009; 30:733–738.

39 de Vries LS, Eken P, Dubowitz LM: The spectrum of leukomalacia using cranial ultrasound. *Behav Brain Res* 1992; 49:1–6.

40 Papile LA, Burstein J, Burstein R, Koffler H: Incidence and evolution of subependymal and intraventricular hemorrhage: a study of infants with birth weights less than 1,500 gm. *J Pediatr* 1978; 92:529–534.

41 Jobe AH, Bancalari E: Bronchopulmonary dysplasia. *Am J Respir Crit Care Med* 2001; 163:1723–1729.

42 Walsh MC, Kliegman RM: Necrotizing enterocolitis: treatment based on staging criteria. *Pediatr Clin North Am* 1986; 33:179–201.

43 Plummer CP: Evaluation of maternal and neonatal outcomes after maintenance tocolysis: a retrospective study. *J Obstet Gynaecol Res* 2012; 38:198–202.

44 Yaju Y, Nakayama T: Effectiveness and safety of ritodrine hydrochloride for the treatment of preterm labour: a systematic review. *Pharmacoepidemiol Drug Saf* 2006; 15:813–822.

45 Guerrini A, Mancini I, Maietti S, Rossi D, Poli F, Sacchetti G, Gambari R, Borgatti M: Expression of pro-inflammatory interleukin-8 is reduced by ayurvedic decoctions. *Phytother Res* 2014; 28:1173–1181.

46 Quan J, Liu J, Gao X, Liu J, Yang H, Chen W, Li W, Li Y, Yang W, Wang B: Palmitate induces interleukin-8 expression in human aortic vascular smooth muscle cells via Toll-like receptor 4/nuclear factor-κB pathway (TLR4/NF-κB-8). *J Diabetes* 2014; 6:33–41.

47 Cielecka-Kuszyk J, Siennicka J, Jabłońska J, Rek O, Godzik P, Rabczenko D, Madaliński K: Is interleukin-8 an additional to histopathological changes diagnostic marker in HCV-infected patients with cryoglobulinemia? *Hepatol Int* 2011; 5:934–940.

48 Ito M, Nakashima A, Hidaka T, Okabe M, Bac ND, Ina S, Yoneda S, Shiozaki A, Sumi S, Tsuneyama K, Nikaido T, Saito S: A role for IL-17 in induction of an inflammation at the fetomaternal interface in preterm labour. *J Reprod Immunol* 2010; 84:75–85.

49 Luo L, Ibaragi T, Maeda M, Nozawa M, Kasahara T, Sakai M, Sasaki Y, Tanebe K, Saito S: Interleukin-8 levels and granulocyte counts in cervical mucus during pregnancy. *Am J Reprod Immunol* 2000; 43:78–84.

50 Holst RM, Hagberg H, Wennerholm UB, Skogstrand K, Thorsen P, Jacobsson B: Prediction of spontaneous preterm delivery in women with preterm labor: analysis of multiple proteins in amniotic and cervical fluids. *Obstet Gynecol* 2009; 114: 268–277.

51 Keeler SM, Kiefer DG, Rust OA, Vintzileos A, Atlas RO, Bornstein E, Hanna N: Comprehensive amniotic fluid cytokine profile evaluation in women with a short cervix: which cytokine(s) correlates best with outcome? *Am J Obstet Gynecol* 2009; 201:276. e1-6.

52 Yoneda S, Shiozaki A, Yoneda N, Shima T, Ito M, Yamanaka M, Hidaka T, Sumi S, Saito S: Prediction of exact delivery time in patients with preterm labor and intact membranes at admission by amniotic fluid interleukin-8 level and preterm labor index. *J Obstet Gynaecol Res* 2011; 37:861–866.

53 Coultrip LL, Lien JM, Gomez R, Kapernick P, Khoury A, Grossman JH: The value of amniotic fluid interleukin-6 determination in patients with preterm labor and intact membranes in the detection of microbial invasion of the amniotic cavity. *Am J Obstet Gynecol* 1994; 171:901–911.

54 Romero R, Yoon BH, Mazor M, Gomez R, Diamond MP, Kenney JS, Ramirez M, Fidel PL, Sorokin Y, Cotton D: The diagnostic and prognostic value of amniotic fluid white blood cell count, glucose, interleukin-6, and gram stain in patients with preterm labor and intact membranes. *Am J Obstet Gynecol* 1993; 169: 805–816.

J Med Ultrasonics (2015) 42:113–116
DOI 10.1007/s10396-014-0561-9

CASE REPORT

Prenatal diagnosis of enterolithiasis at 18 weeks: multiple foci of intraluminal calcified meconium within echogenic bowel

Arihiro Shiozaki · Satoshi Yoneda · Takashi Iizuka · Tae Kusabiraki · Masami Ito · Mika Ito · Noriko Yoneda · Hideo Yoshimoto · Shigeru Saito

Received: 8 January 2014 / Accepted: 23 June 2014 / Published online: 30 July 2014

Abstract Enterolithiasis is an uncommon finding of a dilated hyperechogenic bowel with multiple ball-like echogenic structures at a routine prenatal check-up using ultrasonography. We here report a case of prenatally diagnosed enterolithiasis at 18 weeks of gestation, showing multiple hyperechogenic foci rolling within the bowel fluid after peristalsis. The size of the dilated bowel gradually increased during pregnancy. Magnetic resonance image demonstrated the dilated lower bowel with blind-ending rectum. A postnatal contrast medium study with retrograde urethrography revealed a middle imperforate anus and a rectourethral fistula. A careful examination, even before 20 weeks of gestation, is extremely useful in demonstrating intraluminal coarse calcifications within an echogenic bowel.

Keywords Echogenic bowel · Enterolithiasis · Imperforate anus · Intraluminal calcification · Rectourethral fistula

Introduction

Enterolithiasis is one of the fetal abnormalities of the anorectal region. It is relatively rare and difficult to diagnose sonographically. A rectourinary fistula can be associated with an imperforate anus, leading to the intraluminal mixing of fetal urine and meconium during pregnancy. We report here the first case of the prenatal sonographic diagnosis of enterolithiasis with movement of enteroliths in a dilated echogenic bowel at 18 weeks of gestation in the English language in Japan.

A. Shiozaki · S. Yoneda · T. Kusabiraki · Masami Ito · Mika Ito · N. Yoneda · S. Saito (✉)
Department of Obstetrics and Gynecology, University of Toyama, 2630 Sugitani, Toyama 930-0194, Japan
e-mail: s30saito@med.u-toyama.ac.jp

T. Iizuka · H. Yoshimoto
Department of Obstetrics and Gynecology, Saiseikai Takaoka Hospital, 387-1 Futazuka, Takaoka 933-8525, Japan

Case report

A 36-year-old, gravida 4, para 1, Japanese woman without significant medical history presented for a routine prenatal check-up at 18 weeks 5 days of gestation. Sonography examination using a Voluson E6 ultrasound machine (GE Healthcare Ultrasound, Milwaukee, WI, USA) with a 2.0–5.0-MHz probe demonstrated that the fetal growth was appropriate for 18 weeks of gestation. The fetal lower abdomen contained multiple coarse hyperechoic foci, which were 2–3 mm in diameter, within a dilated loop of hyperechogenic bowel between the urinary bladder and the sacrum. When peristalsis in this segment was present, the multiple foci were rolling within the bowel fluid (Fig. 1a). She was referred to our hospital for further evaluation at 18 weeks and 6 days. The fetal biometry was appropriate for gestational age, and a normal amount of amniotic fluid was observed. In addition, the fetus had no ascites or extraluminal calcified meconium. The sex of the fetus seemed to be female because of pudendal cleavage. A possible diagnosis of anorectal malformation with rectourinary fistula was made.

Ultrasound examination

Follow-up ultrasound examinations showed the persistence of echogenic foci within the dilated colon and rectum (Fig. 1b, c). The size of the hyperechogenic bowel gradually increased from 3.2 × 1.2 cm (28 weeks and 6 days,

Fig. 1 Sonographic appearance of the dilated bowel with hyperechogenic bowel wall (*arrows*) (**a**) at 18 weeks and 5 day. The foci were moving in the bowel with peristalsis, **b** at 28 weeks and 6 days, **c** at 32 weeks and 5 days, and **d** at day 6 after delivery

Fig. 1b) to 4.2 × 1.1 cm (32 weeks and 5 days, Fig. 1c). At 6 days after birth, the dilated bowel with echogenic foci was still seen (Fig. 1d).

Magnetic resonance imaging

To further rule out anorectal malformation, MRI was performed at 37 weeks and 0 day. It demonstrated a dilated bowel (sigmoid colon and rectum) with enterolithiasis (Fig. 2). The external genitalia showed ambiguity when a phallus-like structure could be visualized.

The patient delivered a male, weighing 2,338 g (−1.2 SD), at 37 weeks and 1 day after induction of labor because of decreased variability. External genital examination showed a phallus with bifid scrotum and no anal opening.

Retrograde cystography

Postnatal retrograde cystography showed a rectourethral fistula and an imperforate anus (Fig. 3).

Colostomy was performed at the second day of life. The following course was uneventful. The baby was discharged on the 34th day.

Discussion

Enterolithiasis is a rare entity. Prenatal detection of fetal intraluminal calcifications using ultrasound, even if in a routine check-up, suggests the possibility of anorectal malformation [1–6]. Once the diagnosis of echogenic

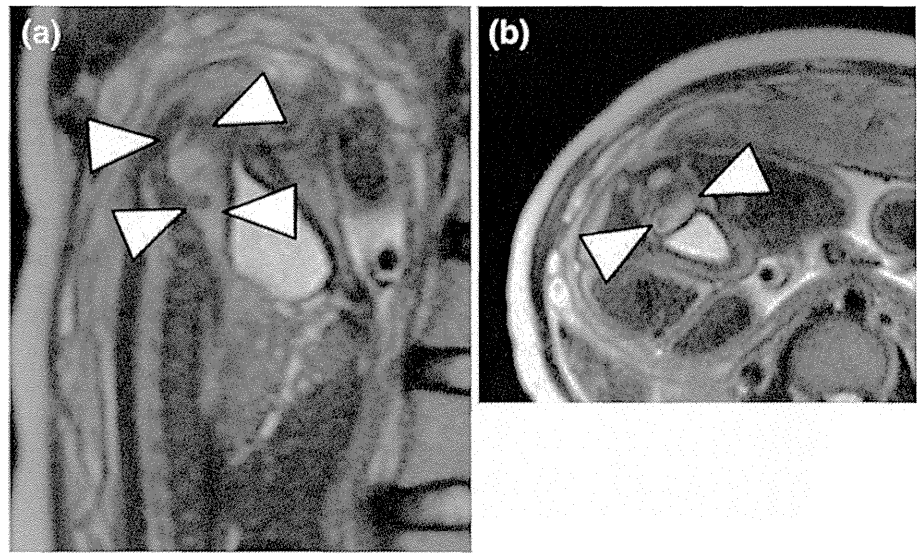

Fig. 2 Magnetic resonance imaging (MRI) at 37 weeks and 0 day (**a**, **b**). A dilated (7.3 × 1.6 cm), spindle-shaped lower bowel (sigmoid to rectum) was seen behind the urinary bladder (*arrowheads*). Ball-like structures (slightly low intensity, *arrowhead*) seemed to float in the intestinal fluid (slightly high intensity) within the blind-ending rectum

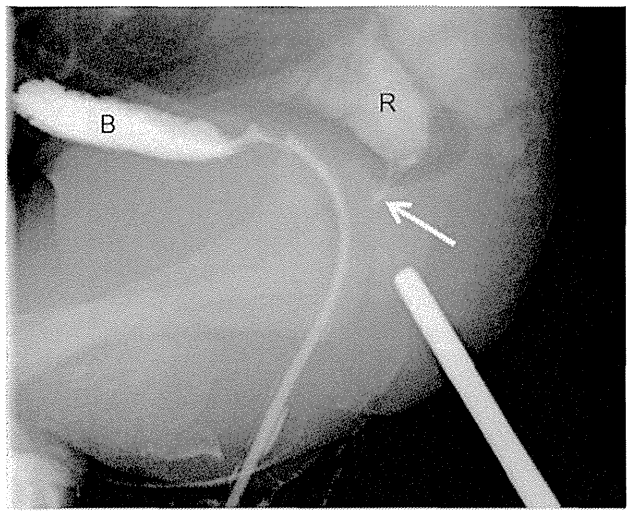

Fig. 3 A contrast medium study with retrograde urethrography exhibited a rectourethral fistula (*arrow*). Contrast medium easily moved to the rectum through the rectourethral fistula. *B* urinary bladder, *R* rectum

bowel is made, a thorough ultrasound examination of the fetal anatomy is warranted as follows: assessment of amniotic fluid, placenta, and membranes, including intra-amniotic bleeding such as particulate debris floating in the amniotic fluid, chorio-amniotic separation, and echogenic material in the fetal stomach [7].

Pohl-Schckinger et al. [5] found that a rectourinary fistula was present in 82 % of 48 cases with anorectal malformation and enterolithiasis, and they concluded that the prenatal diagnosis of enterolithiasis and lower bowel obstruction should alert practitioners to the likely risk of an additional rectourinary fistula. We agree with their finding, and this is an important milestone in cases of enterolithiasis.

Although the mechanisms of calcification of intraluminal meconium are poorly understood, Shimotake et al. [8] suggested that the intraluminal meconium calculi were derived from meconium and fetal urine, using infrared spectroscopic analysis. Therefore, it is suggested that the stasis of meconium due to the lower segment obstruction of the colon (imperforate anus) and the urine-meconium mixing by an enterourinary fistula (rectourinary fistula, rectovesical fistula, rectourethral fistula, vesicovaginorectal fistula) [5] are important key factors for the mechanism of intraluminal calcifications.

Berdon et al. [9] reported five cases of calcified intraluminal meconium in newborns with rectourinary fistulae associated with imperforate anus. And they found that, after adding these five cases to the previously published three cases without meconium peritonitis, all eight cases were male. On the contrary, Anderson et al. [10] reported one female case of enterolithiasis associated with anorectal malformation and commented that the Müllerian system was not sufficiently developed to interpose between the rectum and urinary tract.

A limitation of this report is that we could not evaluate the "ball-like echogenic structures" in the rectum. We could not send them for pathological examination because they had been discarded after the operation.

In conclusion, this case report is the first case report of prenatal diagnosis of enterolithiasis at 18 weeks of gestation in the English language in Japan. When moving hyperechogenic structures within distended bowel are recognized by ultrasonography anytime during pregnancy, we should suspect the presence of enterolithiasis with an imperforate anus and a rectourinary fistula.

Conflict of interest The authors report no conflict of interest.

Ethical standard All procedures followed were in accordance with the ethical standards of the responsible committee on human experimentation (institutional and national) and with the Helsinki Declaration of 1975, as revised in 2008 (5). Informed consent was obtained from this patient for being included in the study.

References

1. Shalev E, Weiner E, Zuckerman H. Prenatal ultrasound diagnosis of intestinal calcifications with imperforate anus. Acta Obstet Gynecol Scand. 1983;62:95–6.
2. Mandell J, Lillehei CW, Greene M, et al. The prenatal diagnosis of imperforate anus with rectourinary fistula: dilated fetal colon with enterolithiasis. J Pediatr Surg. 1992;27:82–4.
3. Achiron R, Daniel Y, Levran D, et al. Fetal enterolithiasis and anhydramnios; due to in utero hepatorenal syndrome? Prenat Diagn. 1998;18:1195–7.
4. Lubusky M, Prochazka M, Dhaifalah I, et al. Fetal enterolithiasis: prenatal sonographic and MRI diagnosis in two cases of urorectal septum malformation (URSM) sequence. Prenat Diagn. 2006;26:345–9.
5. Pohl-Schickinger A, Henrich W, Degenhardt P, Bassir C, Hüseman D, et al. Echogenic foci in the dilated fetal colon may be associated with the presence of a rectourinary fistula. Ultrasound Obstet Gynecol. 2006;28:341–4.
6. Rolle U, Faber R, Robel-Tillig E, et al. Bladder outlet obstruction causes fetal enterolithiasis in anorectal malformation with rectourinary fistula. J Pediatr Surg. 2008;43:e11–3.
7. Sepulveda W, Sebire NJ. Fetal echogenic bowel: a complex scenario. Ultrasound Obstet Gynecol. 2000;16:510–4.
8. Shimotake T, Higuchi K, Tsuda T, et al. Infrared spectrophotometry of intraluminal meconium calculi in a neonate with imperforate anus and rectourethral fistula. J Pediatr Surg. 2006;41:1173–6.
9. Berdon WE, Baker DH, Wigger HJ, et al. Calcified intraluminal meconium in newborn males with imperforate anus. Enterolithiasis in the newborn. Am J Roentgenol Radium Ther Nucl Med. 1975;125:449–55.
10. Anderson S, Savader B, Barnes J, et al. Enterolithiasis with imperforate anus. Report of two cases with sonographic demonstration and occurrence in a female. Pediatr Radiol. 1988;18:130–3.

Journal of Reproductive Immunology 107 (2015) 10–19

Contents lists available at ScienceDirect

Journal of Reproductive Immunology

journal homepage: www.elsevier.com/locate/jreprimm

Helios-positive functional regulatory T cells are decreased in decidua of miscarriage cases with normal fetal chromosomal content

Kumiko Inada, Tomoko Shima, Mika Ito, Akemi Ushijima, Shigeru Saito*

Department of Obstetrics and Gynecology, University of Toyama, Toyama 930-0194, Japan

ARTICLE INFO

Article history:
Received 10 June 2014
Received in revised form 9 September 2014
Accepted 10 September 2014

Keywords:
Effector Treg
Helios
Human pregnancy
Miscarriage
Naturally occurring Treg

ABSTRACT

Regulatory (Treg) T cells play essential roles in the maintenance of allogeneic pregnancy in mice and humans. Recent data show that Foxp3 expression occurs in both immunosuppressive Treg and -nonsuppressive effector T (Teff) cells upon activation in humans. Samstein et al. (2012) reported that inducible Treg (iTreg) cells enforce maternal–fetal tolerance in placental mammals. Therefore, we should reanalyze which types of Treg cell play an important role in the maintenance of allogeneic pregnancy. In this study, we studied the frequencies of naïve Treg cells, effector Treg cells, Foxp3$^+$ Teff cells, Helios$^+$ naturally occurring Treg (nTreg) cells, and Helios$^-$ iTreg cells using flow cytometry. The frequencies of effector Treg cells and Foxp3$^+$ Teff cells among CD4$^+$Foxp3$^+$ cells in the decidua of miscarriage cases with a normal embryo karyotype ($n=8$) were significantly lower ($P=0.0105$) and significantly higher ($P=0.0258$) than those in normally progressing pregnancies ($n=11$), respectively. However, these frequencies in miscarriages with an abnormal embryo karyotype ($n=15$) were similar to those in normally progressing pregnancies. The frequencies of these cell populations in the three groups were unchanged in peripheral blood; on the other hand, most of the effector Treg cells in the decidua were Helios$^+$ nTreg cells and these frequencies were significantly higher than those in peripheral blood, while those among effector Treg and naïve Treg cells in the decidua and peripheral blood were similar among the three groups. These data suggest that decreased Helios$^+$ effector nTreg might play an important role in the maintenance of pregnancy in humans.

1. Introduction

Regulatory T cells (Treg) play an important role in the induction and maintenance of tolerance (Sakaguchi et al., 1995; Sakaguchi, 2005). In 2004, Aluvihare et al. and our group first reported that Treg cells might mediate maternal tolerance to the fetus in mice and humans (Aluvihare et al., 2004; Sasaki et al., 2004). Since then, many lines of evidence supporting the importance of Treg cells in the implantation period and the early pregnancy period have been presented, with more detailed characterization of Treg cells in mice (Zenclussen et al., 2005, 2006; Darrasse-Jèze et al., 2006; Kallikourdis et al., 2007; Robertson et al., 2009; Shima et al., 2010; Kahn and Baltimore, 2010; Guerin et al., 2011; Rowe et al., 2011, 2012; Samstein et al., 2012; Yin et al., 2012) and in humans (Tilburgs et al., 2008, 2009; Sasaki et al., 2007; Yang et al., 2008; Jin et al., 2009; Mei et al., 2010; Wang et al., 2010, 2011; Winger and Reed, 2011; Lee et al., 2011; Steinborn et al., 2012).

For example, adoptive transfer of Treg cells purified from normal pregnant mice prevented fetal loss in CBA/J♀ × DBA/2J ♂ mice (Zenclussen et al., 2005; Yin et al.,

* Corresponding author. Tel.: +81 76 434 7355; fax: +81 76 434 5036.
E-mail address: s30saito@med.u-toyama.ac.jp (S. Saito).

http://dx.doi.org/10.1016/j.jri.2014.09.053
0165-0378/

2012), suggesting that fetal antigen-specific Treg cells might play essential roles in the maintenance of allogeneic pregnancy. Seminal plasma plays an important role in the expansion of fetal antigen-specific Treg (Robertson et al., 2009; Guerin et al., 2011). Memory Treg cells that recognize paternal antigens also rapidly increase in a second pregnancy with the same partner compared with the first (Rowe et al., 2012). A decreased Treg cell pool was observed in recurrent miscarriage cases in humans (Yang et al., 2008; Jin et al., 2009; Mei et al., 2010; Wang et al., 2010, 2011; Lee et al., 2011) and a low Treg cell level predicts the risk of miscarriage in cases of unexplained recurrent pregnancy loss (Winger and Reed, 2011). Selective migration of fetus-specific Treg cells from the peripheral blood to the decidua in human pregnancy has also been reported (Tilburgs et al., 2008). We have reported that the population of $CD4^+Foxp3^+$ Treg cells at the decidua basalis in miscarriage with a normal karyotype embryo was significantly lower than in normally progressing pregnancy and in miscarriage with an abnormal embryo, suggesting that dysregulation of maternal tolerance to the fetus might be associated with unknown etiology of miscarriage in humans (Inada et al., 2013).

We considered that Foxp3 is the most reliable marker for Treg cells (Hori et al., 2003), but recent data have shown that $Foxp3^+$ expression in humans occurs in both immunosuppressive Treg cells and non-suppressive and cytokine-producing effector T cells (Walker et al., 2003; Gavin et al., 2006; Allan et al., 2007). Miyara et al. (2009) reported that human $CD4^+Foxp3^+$ cells are classified into $CD4^+CD45RA^+Foxp3^{low}$ naïve Treg cells, $CD4^+CD45RA^-Foxp3^{high}$ effector Treg cells, and $CD4^+CD45RA^-Foxp3^{low}$ effector T (Teff) cells. Importantly, those $Foxp3^+$ Teff cells have no capacity for immunoregulation. $CD4^+CD25^{bright}$ T cells exhibit regulatory function in humans (Beacher-Allan et al., 2001). Miyara et al. (2009) showed that $CD4^+CD25^{bright}$ cells are composed of $CD4^+CD45RA^+Foxp3^{low}$ naïve T cells, $CD4^+CD45RA^-Foxp3^{low}$ Teff cells, and $CD4^+CD45RA^-Foxp3^{high}$ effector Treg cells. $CD4^+CD25^+CD127^-$ cells are believed to be a reliable marker for Treg cells (Seddiki et al., 2006), but Kleinewietfeld et al. (2009) pointed out that some of the $CD4^+CD25^+CD127^-$ cells are Teff cells, which produce IFN-γ, IL-2, and IL-17. These findings suggest that we should re-evaluate which subsets of $Foxp3^+$ cells play an important role in the maintenance of pregnancy.

Treg cells are classified as naturally occurring Treg (nTreg) generated in the thymus and inducible T (iTreg) generated in the periphery (Sakaguchi, 2005). Samstein et al. (2012) reported that conserved noncoding sequence 1 (CNS1), which is essential for iTreg differentiation, is conserved only in placental mammals, and CNS1-deficient female mice showed increased fetal resorption in allogeneic pregnancy. These findings suggest that iTreg induction at the fetomaternal interface might be important for a successful pregnancy in placental mammals.

However, it has still not been reported which subset of Treg cells is important for the maintenance of human pregnancy: naive Treg cells, effector Treg cells, nTregs or iTregs. As such, we have studied the populations of naïve Treg cells, effector Treg cells, $Foxp3^+$ Teff cells, $Helios^+$ nTreg cells, and $Helios^-$ iTreg cells in the decidua or peripheral blood of miscarriage cases with abnormal or normal fetal chromosomal content.

2. Materials and methods

2.1. Cases of normal pregnancy and miscarriage

This study was approved by the Ethics Committee of the University of Toyama. We obtained written informed consent from all the cases. We enrolled 11 subjects with normally progressing pregnancy, 15 with miscarriage and an abnormal embryo karyotype (trisomy [$n=14$] including trisomy8 [$n=2$], trisomy13 [$n=2$], trisomy15 [$n=1$], trisomy16 [$n=3$], trisomy21 [$n=3$], trisomy22 [$n=3$], and translocation [$n=1$]), and 8 with miscarriage and a normal embryo karyotype. Chorionic villi were sampled from miscarriage cells for cytogenetic analysis. Fetal chromosomal karyotyping was performed by conventional G-band staining. Echo sonography was performed every two weeks, and patients were advised to obtain an induced abortion if the fetal heartbeat ceased or was never detected. In women with a normally progressing pregnancy, fetal heartbeat was identified before elective termination. None of the subjects had any risk factors such as genetic abnormalities (neither themselves nor their husband), uterine malformation, thyroid dysfunction or anti-phospholipid antibody syndrome.

The clinical background in these groups is shown in Table 1. The numbers of previous miscarriages in women miscarrying with an abnormal embryo and miscarrying with a normal embryo were significantly higher than in the normal pregnancy group. Gestational weeks at sampling, body mass index (BMI), and frequency of smoking were similar among the three groups.

2.2. Flow cytometry

Decidual mononuclear cells (leukocytes) were purified by the Ficoll Hypaque method after homogenization and filtration through a 32-μm nylon mesh, as previously reported (Saito et al., 1992).

The following monoclonal antibodies (mAbs) were used in this study: anti-CD4 (Per CP-Cy5.5; BD Biosciences, NJ, USA), anti-CD45RA (Biotin; BD Bioscience), and streptavidin labeled with APC-Cy7 (BD Biosciences) as cell surface markers, and anti-Foxp3 (FITC; eBioscience, San Diego, CA, USA) and anti-Helios (Alexa Fluor 647; eBioscience) as intracellular markers. Decidual and peripheral mononuclear cells were first stained with anti-CD4 mAb and anti-CD45RA mAb for 30 min on ice. Cells were washed with phosphate-buffered saline (PBS) three times. Next, APC-Cy7-labeled streptavidin was added and inoculated for 15 min on ice. After washing the cells with PBS three times, they were fixed and permeabilized by incubation for 30 min with fixation/permeabilization buffer (eBioscience), and then stained with anti-Foxp3 and anti-Helios mAb. Flow cytometry analysis was performed on a BD FACScanII (BD Biosciences).

Lymphocytes were gated based on both forward and side scatter parameters (Fig. 1, left). Monocytes,

Table 1
Clinical background in normal pregnancy, miscarriage with an abnormal embryo and miscarriage with a normal embryo.

	Normal pregnancy $n=11$	Miscarriage with an abnormal embryo $n=15$	Miscarriage with a normal embryo $n=8$
Age (year)*	27.5 ± 0.7 (16–39)	37.3 ± 0.3 (29–44)†	32.1 ± 0.8 (22–42)
Gravidities*,**	1.0 ± 0.1 (0–2)	2.2 ± 0.08 (0–4)†	2.5 ± 0.2 (0–5)
Nulliparity	6/11 (54.5%)	10/15 (66.7%)	4/8 (50.0%)
No. of liveborn children*	0.7 ± 0.08 (0–2)	0.3 ± 0.03 (0–1)	0.5 ± 0.07 (0–1)
No. of miscarriages*,***	0 (0–0)	2.5 ± 0.08 (1–5)†††	2.8 ± 0.2 (1–5)††
Stillbirth*	0 (0–0)	0.1 ± 0.02 (0–1)	0 (0–0)
Gestational weeks*	7.5 ± 0.2 (6–10)	7.2 ± 0.09 (5–10)	6.1 ± 0.2 (5–9)
BMI*	20.4 ± 0.2 (17.7–23.1)	21.8 ± 0.2 (17.7–27.1)	20.6 ± 0.4 (18.0–27.7)
Smoker	3/11 (27.2%)	1/15 (6.7%)	0/8 (0%)

* Mean ± SEM (range).
** This pregnancy or miscarriage is not included in gravidities.
*** This miscarriage is included in no. of miscarriages.
† $P<0.05$ vs. normal pregnancy.
†† $P<0.001$ vs. normal pregnancy.
††† $P<0.0001$ vs. normal pregnancy.

granulocytes, and decidual stromal cells were excluded from the setting of a lymphocyte gate as in Fig. 1 (left). After gating on $CD4^+$ cells (Fig. 1, center), the proportions of $CD4^+CD45RA^+Foxp3^{low}$ naïve Treg, $CD4^+CD45RA^-Foxp3^{high}$ effector Treg, and $CD4^+CD45RA^-Foxp3^{low}$ Teff cells were determined among $CD4^+Foxp3^+$ cells (Fig. 1). Isotype-matched fluorochrome-conjugated mice IgG were used as a control. $Foxp3^{low}$ and $Foxp3^{high}$ were classified as follows. In the peripheral blood, some of the $CD4^+$ cells expressed $Foxp3^{low}$ (Fig. 1, upper column). The expression of Foxp3 in $Foxp3^{high}$ cells was brighter than those in $CD4^+Foxp3^{low}$ cells. In the decidua, $CD4^+Foxp3^{high}$ cells formed a cluster, and we classified these as $CD4^+Foxp3^{high}$ cells and $CD4^+Foxp3^{low}$ cells (Fig. 1, center and right).

2.3. Statistical analysis

Statistical analysis was performed using a statistical software package (SAS version 9.1; SAS Institute, USA). Data were analyzed using the Mann–Whitney U test. A value of $P<0.05$ was considered statistically significant.

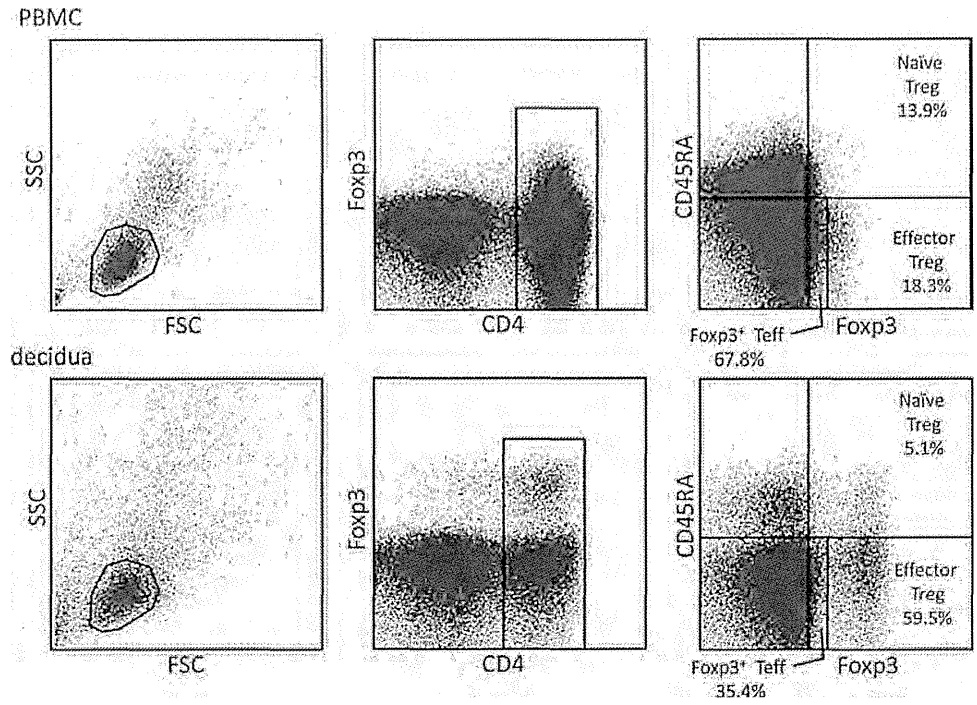

Fig. 1. Gating strategy for the detection of $CD4^+CD45RA^+Foxp3^{low}$ naïve Treg cells, $CD4^+45RA^-Foxp3^{high}$ effector Treg cells, and $CD4^+CD45RA^-Foxp3^{low}$ effector T cells. Lymphocytes in the peripheral blood (upper column) and decidua (lower column) were gated on forward and side scatter parameters. $CD4^+$ T cells in peripheral blood and decidua were classified into $CD45RA^+Foxp3^{low}$ cells, $CD45RA^-Foxp3^{high}$ effector Treg cells, and $CD45RA^-Foxp3^{low}$ Teff cells. The percentages of $CD45RA^+Foxp3^{low}$ cells, $CD45RA^-Foxp3^{high}$ cells, and $CD45RA^-Foxp3^{low}$ cells among $CD4^+Foxp3^+$ T cells are displayed.